Magnetic and non-Fermi-liquid phases in $Ce_{1-x}Y_xRhIn_5$

V. S. Zapf, N. A. Frederick, K. L. Rogers,* K. D. Hof,† P.-C. Ho, E. D. Bauer, and M. B. Maple
Department of Physics and Institute for Pure and Applied Physical Sciences, University of California at San Diego, La Jolla, California 92093-0350

(Received 31 July 2002; revised manuscript received 18 November 2002; published 6 February 2003)

We have investigated single-crystal samples of $Ce_{1-x}Y_xRhIn_5$ by means of specific heat C, magnetic susceptibility χ, and electrical resistivity ρ measurements as a function of temperature T. As yttrium is substituted for cerium, the Néel temperature is suppressed, yielding a quantum critical point at yttrium concentration $x_c \sim 0.38$. Non-Fermi-liquid behavior (NFL) occurs in $C(T)$ and $\chi(T)$ over an extended range of yttrium concentrations above the quantum critical point $0.4 \leqslant x \leqslant 0.9$ with $C(T)$ and $\chi(T)$ displaying power law T dependences at low temperatures. Remarkably, the NFL behavior become more pronounced with increasing distance from the quantum critical point. For the samples with $0.2 \leqslant x \leqslant 0.9$ we also observe features in the specific heat and magnetic susceptibility above T_N that may be due to tetragonal crystalline electric field splitting of the Ce^{3+} $J=5/2$ multiplet with a Γ_7 ground state.

DOI: 10.1103/PhysRevB.67.064405 PACS number(s): 71.10.Hf, 71.27.+a, 71.70.Ch

I. INTRODUCTION

A growing class of heavy fermion intermetallic compounds display non-Fermi-liquid (NFL) behavior, which is characterized by temperature or frequency dependences of the physical properties that deviate from the predictions of Landau Fermi liquid theory at low temperatures.[1,2] For example, the electrical resistivity $\rho(T)$, specific heat $C(T)$, and magnetic susceptibility $\chi(T)$ typically exhibit power law or logarithmic divergences at low temperatures. NFL behavior has been observed in both ternary and pseudoternary compounds under ambient and applied pressures. NFL behavior often appears in the vicinity of a quantum critical point where a magnetic phase transition has been suppressed to zero temperature by pressure or chemical substitution. Although a variety of theories have been advanced to explain NFL behavior, many aspects of these systems continue to elude our understanding.

Recently, a new class of heavy fermion compounds with the formula $CeMIn_5$ (M = Rh, Ir, Co) were discovered[3] that exhibit a variety of ground states including NFL behavior, antiferromagnetism, and superconductivity. The compound $CeRhIn_5$ displays incommensurate antiferromagnetic (AFM) order below a Néel temperature $T_N = 3.8$ K.[4] Like many other heavy fermion systems, such as UPd_2Al_3, and $CePd_2Si_2$,[5–7] the AFM order can be suppressed by applied pressure or chemical substitution. The application of pressure causes a slight suppression of T_N, and the AFM order disappears at 21 kbar, to be replaced with superconductivity with a T_c of 2.2 K.[4] T_N can also be suppressed by substituting Co or Ir for Rh.[8,9] In these cases, superconductivity occurs on both sides of the quantum critical point where T_N is suppressed to zero, and superconductivity coexists with antiferromagnetism for a wide range of Rh concentrations. The end member compounds $CeCoIn_5$ and $CeIrIn_5$ are both superconductors with bulk T_c's of 2.2 K and 0.4 K, respectively.[10,11] NFL behavior has been observed in all three compounds: $CeRhIn_5$, $CeCoIn_5$, and $CeIrIn_5$.[12,13] However, the appearance of superconductivity at a relatively high temperature complicates the investigation of NFL behavior, which can only be observed above T_c or in applied magnetic fields high enough to suppress the superconductivity. In this paper, we investigate the effect of yttrium substitution for cerium in $CeRhIn_5$. The Néel temperature is suppressed with increasing yttrium, giving rise to a quantum critical point at $\sim$38% yttrium concentration. We observe no superconducting transitions in the measured temperature range, which allows us to make a detailed study of NFL behavior down to low temperatures and over a wide range of yttrium concentrations above the quantum critical point.

II. EXPERIMENTAL DETAILS

Single crystals of $Ce_{1-x}Y_xRhIn_5$ were grown using an indium flux method in alumina crucibles, as described previously.[8] The magnetization M of the crystals was measured as a function of temperature T using a commercial superconducting quantum interference device (SQUID) magnetometer in an applied magnetic field of 1 kOe. Measurements of the electrical resistivity $\rho(T)$ were performed using a standard four-wire technique at temperatures in the range $1.8\ \text{K} \leqslant T \leqslant 300$ K in a commercial ^{4}He cryostat (Quantum Design Physical Properties Measurement System) with excitation currents of 10 mA at frequencies of 16 Hz. Gold leads were attached to the samples with silver epoxy (Epotek H20E). Resistivity between 50 mK and 2.5 K was measured in a ^{3}He-^{4}He dilution refrigerator with a 100 μA excitation current in magnetic fields up to 8 T. Both the current and the magnetic field were applied along the *ab* plane. The specific heat C was measured as a function of temperature between 0.6 and 70 K in a ^{3}He semiadiabatic calorimeter using a standard heat pulse technique.

III. RESULTS

A. Lattice parameters

X-ray powder diffraction measurements reveal that the $Ce_{1-x}Y_xRhIn_5$ single crystals form in the tetragonal $HoCoGa_5$ structure. The lattice parameters a and c were determined from a least-squares fit of the peak positions in the

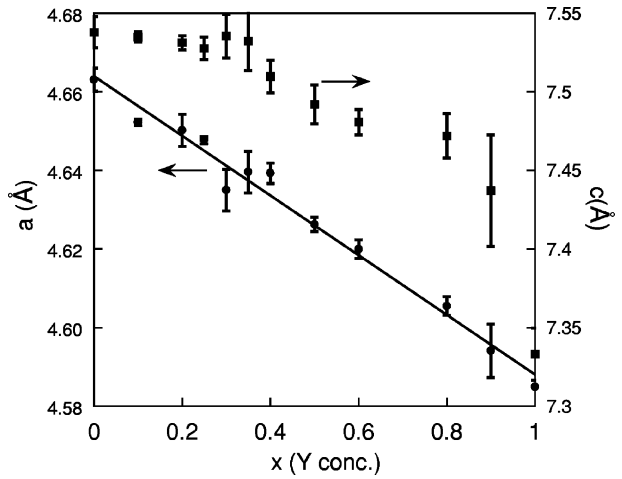

FIG. 1. Tetragonal lattice parameters a and c vs yttrium concentration x for the $Ce_{1-x}Y_xRhIn_5$ system. The straight line is a linear fit to the a vs x data.

x-ray powder diffraction pattern and are shown in Fig. 1. The a parameter contracts linearly with x as the smaller yttrium atom is substituted onto the cerium site, in accordance with Vegard's law. The c parameter varies almost parabolically with x, dropping off very rapidly for $x>0.8$. The more complicated variation of c with x reflects the fact that along the c axis of the crystal the cerium atoms are farther apart, separated by intervening layers of rhodium atoms.

B. Specific heat

The cerium contribution to the specific heat C_m of the $Ce_{1-x}Y_xRhIn_5$ samples with $0\leqslant x\leqslant 0.9$ is shown in Fig. 2, plotted as C_m/T. The lattice contributions were removed by subtracting the lattice specific heat of the isostructural nonmagnetic compound $YRhIn_5$. The sample with $x=0$ ($CeRhIn_5$) shows a sharp peak at $T=3.8$ K which is attributed to the onset of antiferromagnetic order. The presence of spiral antiferromagnetic order at the same temperature in $CeRhIn_5$ has been confirmed by neutron diffraction and[115]In nuclear quadrupole measurements.[14,15] The temperature of this peak in C_m/T at the Néel temperature is suppressed with increasing yttrium concentration, appearing at $T_N=3$ K for $x=0.2$, $T_N=1.5$ K for $x=0.3$, and $T_N=1.4$ K at $x=0.35$ (not shown). The samples with $x\geqslant 0.4$ show no indication of antiferromagnetic order in the specific heat above $T=0.6$ K.

For the samples with $0.4\leqslant x\leqslant 0.9$, $C_m(T)/T$ diverges at the lowest temperatures, suggestive of NFL behavior. However, the analysis of NFL behavior in the specific heat is complicated by the presence of an additional broad feature in the C_m/T vs T data at $T\sim 4$ K. This feature occurs in all the of samples containing both cerium and yttrium, and could result from a Schottky anomaly due to splitting of the Ce^{3+} $J=5/2$ multiplet by tetragonal crystal fields. The analysis of this feature and the NFL behavior are discussed in the next sections.

The specific heat of the $Ce_{1-x}Y_xRhIn_5$ samples contains multiple contributions: heavy fermion behavior, peaks due to antiferromagnetic ordering ($x<0.4$), possible Schottky anomalies, and NFL divergence at low temperatures ($x\geqslant 0.4$). It is noteworthy that the area under all of the C_m/T curves integrated to 6 K is roughly equal. This is shown in Fig. 2(b) in which the entropy S is plotted versus temperature for samples with $0\leqslant x\leqslant 0.8$. For all of the samples containing yttrium, the entropy versus temperature curves converge by 6 K. Thus, it appears that the same heavy electrons are participating in these diverse phenomena: heavy fermion behavior, antiferromagnetic ordering, possible crystalline electric field (CEF) splittings of the Ce^{3+} Hund's rule multiplet, and NFL behavior. The exception is the $CeRhIn_5$ sample whose entropy at 6 K is somewhat smaller than that of the other samples. The reduced entropy in $CeRhIn_5$ could be due to larger CEF splittings of the Ce^{3+} Hund's rule multiplet in this compound.

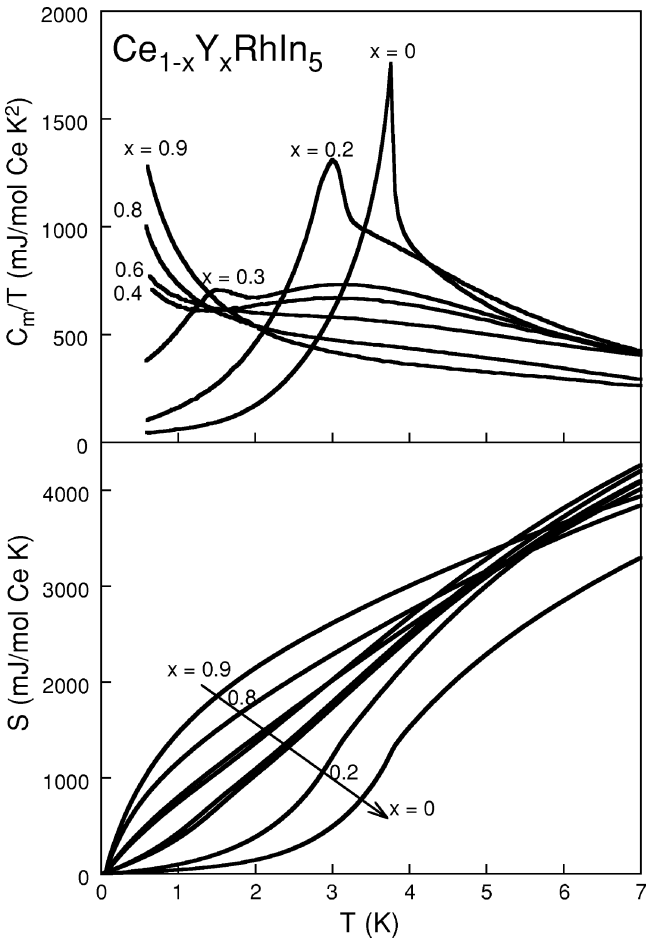

FIG. 2. (a) Magnetic contribution to the specific heat C_m divided by temperature T vs T, normalized per mol of cerium, for samples of $Ce_{1-x}Y_xRhIn_5$ with $0\leqslant x\leqslant 0.9$. (b) Entropy S vs temperature T for samples with $x=0.9$, 0.8, 0.6, 0.4, 0.35, 0.3, 0.2, and 0. The specific heat was extrapolated to zero temperature in order to calculate the entropy.

C. CEF analysis

The specific heat C and magnetic susceptibility χ_{ab} in the ab plane of the $Ce_{1-x}Y_xRhIn_5$ samples with $0.2\leqslant x\leqslant 0.9$

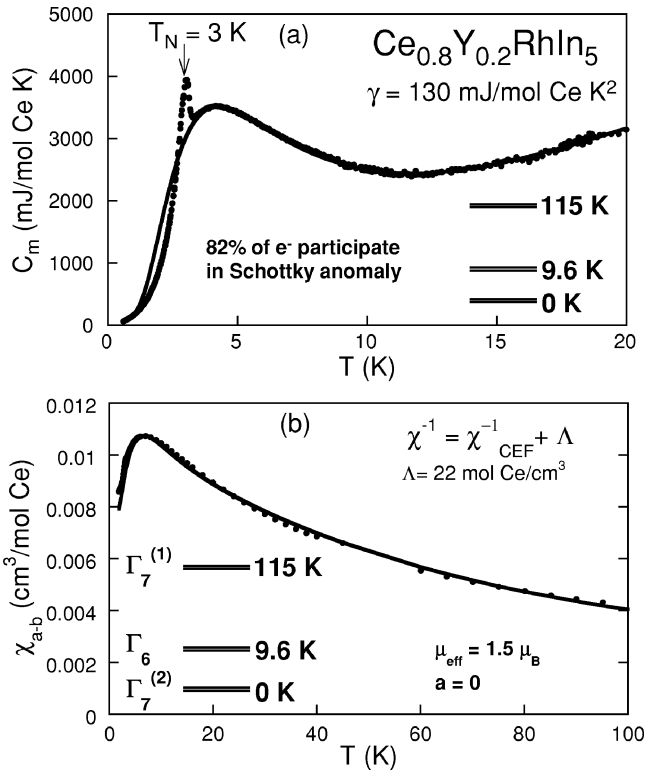

FIG. 3. (a) Magnetic contribution to the specific heat C_m vs temperature T for the sample of $Ce_{1-x}Y_xRhIn_5$ with $x=0.2$. The line is a fit of a Schottky anomaly to the data with energy splittings as shown, reduced to 82%. An electronic specific heat term γT with $\gamma=130$ mJ/mol K^2 was also included in the fit. (b) Magnetic susceptibility in the *ab* plane, χ_{ab}, vs T. The line is a fit of a tetragonal CEF model prediction with parameters as shown.

exhibit rounded features above T_N. One possible explanation for these features is CEF splitting of the Ce^{3+} Hund's rule multiplet. The Ce^{3+} $J=5/2$ multiplet consists of six degenerate energy levels that are split by a tetragonal crystal field into a magnetic Γ_6 doublet and two magnetic Γ_{t7} doublets,[16] where

$$\Gamma_6 = \pm|1/2\rangle,$$
$$\Gamma_{t7}^{(1)} = a|\pm 5/2\rangle - b|\pm 3/2\rangle,$$
$$\Gamma_{t7}^{(2)} = b|\pm 5/2\rangle + a|\pm 3/2\rangle. \quad (1)$$

Accordingly, the specific heat was fit by a Schottky anomaly consisting of three doublets, where the excited-state doublets are located at energies E_1 and E_2 above the ground-state doublet. An electronic contribution γT to the specific heat was also included in the fit. The results for the sample with $x=0.2$ are shown in Fig. 3(a). The best fit to the data yields $E_1=9.6$ K, $E_2=115$ K, and $\gamma=130$ mJ/mol K^2. The prediction for $C(T)$ of the Schottky anomaly had to be multiplied by a scaling factor $f=0.82$ in order to fit the data. Note that the data are already normalized per mole Ce, so this factor f represents an additional reduction in the size of the Schottky anomaly. Similar fits were performed for the samples with $0.4 \leqslant x \leqslant 0.9$, with the fitting parameters listed in Table I. For these samples, an additional power law term was added to describe the NFL behavior, which is discussed in the next section. The energy splitting E_1 increases with x to 18 K at $x=0.9$ while the scaling factor decreases to $f=0.09$ for $x=0.9$. Apparently, as x increases, fewer Ce f electrons contribute to the Schottky anomaly.

TABLE I. Parameters from fits to the specific heat $C(T)$ and magnetic susceptibility $\chi_{ab}(T)$ of the form $C(T)/T = fC_{CEF}/T + BT^{-1+\lambda}$ and $\chi_{ab}(T) = \chi_{CEF} + AT^{-1+\lambda}$. The CEF levels are given by $\Gamma_6 = \pm|1/2\rangle$, $\Gamma_{t7}^{(1)} = a|\pm 5/2\rangle - b|\pm 3/2\rangle$, and $\Gamma_{t7}^{(2)} = b|\pm 5/2\rangle + a|\pm 3/2\rangle$. For the sample with $x=0.2$, only the CEF form and not the power law contribution is fit.

	$C(T)$			$\chi_{ab}(T)$			
x	E_1 (K)	E_2 (K)	f	E_{t6} (K)	E_{t71} (K)	a	μ_{eff}^2 (μ_B)
0.2	9.6	115	0.82	9.6	115	0	1.50
0.4	12.0	127	0.28	14.5	127	0	1.23
0.5				14.0	127	0	1.16
0.6	13.0	127	0.16	13.7	127	0	1.07
0.7				14.2	127	0	0.84
0.8	14.5	127	0.19	18.3	127	0	0.58
0.9	18.4	127	0.09				

The CEF contribution to the magnetic susceptibility in the α direction was determined from the following expression:[17]

$$\chi_{CEF}(T) = \frac{N_A g_J^2}{Z\mu_B^2}\left(\sum_i \frac{\beta|M_{ii}|^2}{e^{\beta E_i}} + 2\sum_{i\neq j}\frac{|M_{ij}|^2}{e^{\beta E_i}(E_j - E_i)}\right), \quad (2)$$

where N_A is Avogadro's number, g_J is the Landé g factor, Z is the partition function, M_{ij} is the matrix element of the angular momentum operator J_α between the ith and jth wave functions, and E_i are the energies of the wave functions above the ground state. A mean-field constant Λ was also included for the sample with $x=0.2$ to account for the AFM order, where $\chi^{-1} = \chi_{CEF}^{-1} + \Lambda$.

The best fit to the data for all of the samples consists of a $\Gamma_{t7}^{(2)}$ ground state, a Γ_6 excited state, and a $\Gamma_{t7}^{(1)}$ second excited state. The fit for the sample with $x=0.2$ is shown in Fig. 3(b). Note that the $\chi_{ab}(T)$ data are fit very well by the same energy level scheme as was found for the specific heat. The parameter a is zero—i.e., the ground state is purely $|5/2\rangle$—and $\Lambda = 22$ mol Ce/cm^3. The effective moment μ_{eff} of the Ce ion was found to be $1.5\mu_B$ which is reduced from the Ce^{3+} free ion moment of $2.54\mu_B$. Similar results were found from CEF fits of the samples with $0.4 \leqslant x \leqslant 0.8$. However, χ_{ab} of these samples also contains a power law contribution, which is described in detail in the next section. For the sample with $x=0.9$, the CEF-like contribution is negligible.

D. Non-Fermi-liquid behavior

For the samples with $0.4 \leqslant x \leqslant 0.9$, the specific heat data can be described by the sum of two contributions: a

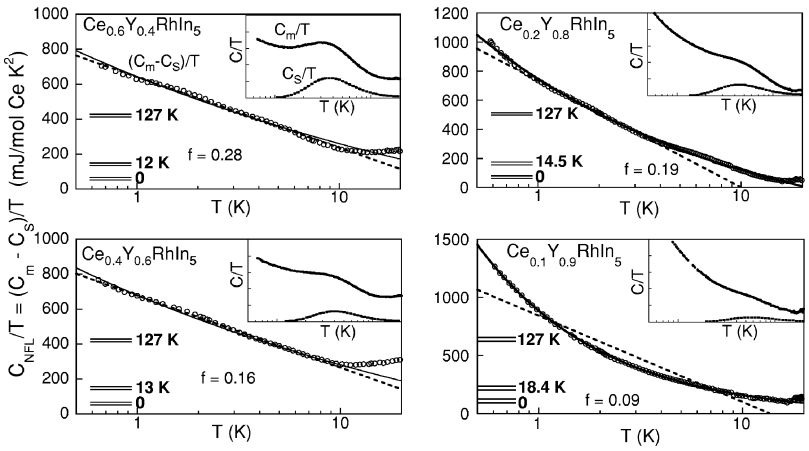

FIG. 4. Non-Fermi-liquid contribution to the specific heat C_{NFL}/T vs temperature T on a semi-logarithmic scale for $Ce_{1-x}Y_xRhIn_5$, where the contribution C_S/T from a Schottky anomaly has been subtracted. The solid lines are fits to the form $C_{\mathrm{NFL}}/T \propto T^n$, and the dashed lines are fits to $C_{\mathrm{NFL}}/T \propto lnT$. The energy level scheme of the Schottky anomalies are given in the lower left-hand corner. The top curves in the insets show the raw C_m/T vs T data on a logarithmic scale, where $C_m = C - C(\mathrm{YRhIn_5})$. Bottom curves in the insets are the assumed Schottky anomaly contributions C_S, which were subtracted to yield the data in the main figure.

Schottky-anomaly-like bump $C_S(T)$ and a low-temperature divergence hereafter referred to as the NFL contribution $C_{\mathrm{NFL}}(T)$. Since most NFL theories predict a power law $[C_{\mathrm{NFL}}(T)/T = \gamma_0 + AT^{-1+\lambda}]$ or logarithmic $[C_{\mathrm{NFL}}(T)/T = \gamma_0 + A \ln T]$ T dependence of $C(T)$, these two forms were used to fit the data. In Fig. 4, $C_{\mathrm{NFL}}(T) = C_m - C_S$ is plotted as $C_{\mathrm{NFL}}(T)/T$ vs $\ln T$. The solid lines are fits to the power law form, and the dashed lines are fits to the logarithmic form. For the samples with $x = 0.4$ and $x = 0.6$, both forms fit the data equally well. However, for the samples with $x = 0.8$ and $x = 0.9$, only the power law describes the data. The power law exponents are given in Table II.

The magnetic susceptibility in the *ab* plane χ_{ab} can also be treated as the sum of a NFL power law T dependence and a CEF contribution. In the inset to Fig. 5, the magnetic susceptibility in the *ab* plane $\chi_{\mathrm{ab}}(T)$ is shown on a log-log scale for samples with $0.4 \leqslant x \leqslant 0.9$. The susceptibility of the samples with $0.4 \leqslant x \leqslant 0.8$ was fit by the expression $\chi_{\mathrm{ab}}(T) = \chi_{\mathrm{CEF}}(T) + AT^{-1+\lambda}$, where the CEF contribution $\chi_{\mathrm{CEF}}(T)$ is given by Eq. (2). In the main part of Fig. 5, the magnetic susceptibility minus the CEF contribution, $\chi_{\mathrm{NFL}}(T) = \chi_{\mathrm{ab}}(T) - \chi_{\mathrm{CEF}}(T)$, is shown on a log-log scale, and the power law fits are solid straight lines. The power law exponent λ is constant at ~ 0.55 for all of the samples, whereas the parameter A increases with increasing x. The CEF parameters and power law exponents λ derived from the fits are listed in Tables I and II. For all of the fits, the ground state is purely $|5/2\rangle$ $(a = 0)$. The energy level splittings in the CEF, E_{t6} and E_{t71}, are close to those determined from the fits of the Schottky anomalies to the specific heat. Also, the magnitude of the CEF-like contribution, reflected by μ_{eff}^2, is reduced with increasing x as was seen in the specific heat. Apparently, the CEF-like contribution to χ_{ab} is suppressed with increasing x as the NFL contribution grows in magnitude. None of the magnetic susceptibility data can be fit by a logarithmic T dependence, which is predicted for the Kondo disorder model.[18]

TABLE II. Parameters of Griffiths phase fits $C/T = \chi_{\mathrm{ab}} = T^{-1+\lambda}$.

x	λ_C	λ_χ
0.4	0.83	0.55
0.5	-	0.54
0.6	0.82	0.53
0.7	-	0.54
0.8	0.66	0.52
0.9	0.30	0.57

The electrical resistivity $\rho(T)$ at low temperatures for samples in the vicinity of the QCP shows some sample dependence which we are in the process of investigating. Varying amounts of filamentary indium would be one possible explanation. Despite the sample dependence, all the $\rho(T)$ data can be fit by power law T dependences $\rho \sim T^n$ with $n < 2$. This is in contrast to the Fermi liquid prediction of $n = 2$. One sample with $x = 0.4$ shows linear-T behavior down to 150 mK. This sample was investigated in detail, over a temperature range of 150 mK to 300 K and in magnetic fields up to 8 T, as shown in Fig. 6. At 0.03 T (the field necessary to suppress the superconductivity of free indium),

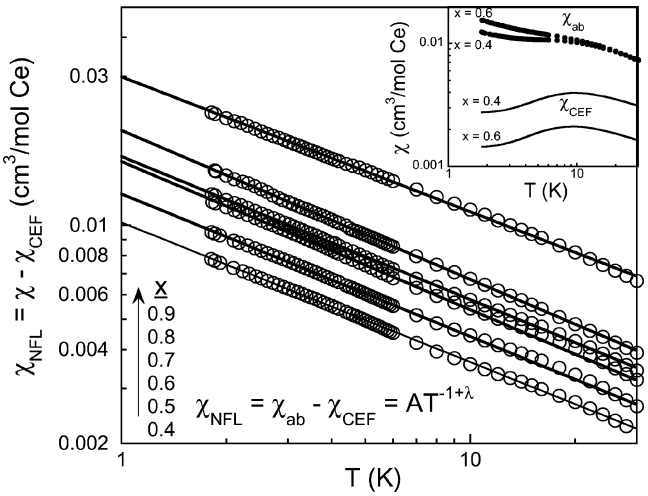

FIG. 5. Inset: data points are raw χ_{ab} vs T data for $x = 0.4$ and $x = 0.6$. Lines are CEF-like contributions $\chi_{\mathrm{CEF}}(T)$, which were subtracted to yield the data in the main figure. Main figure: non-Fermi-liquid contribution to the magnetic susceptibility in the *ab* direction, $\chi_{\mathrm{NFL}}(T) = \chi_{\mathrm{ab}} - \chi_{\mathrm{CEF}}$. The solid lines are fits to a power law $\chi_{\mathrm{NFL}} = AT^{-1+\lambda}$ with $\lambda \sim 0.55$.

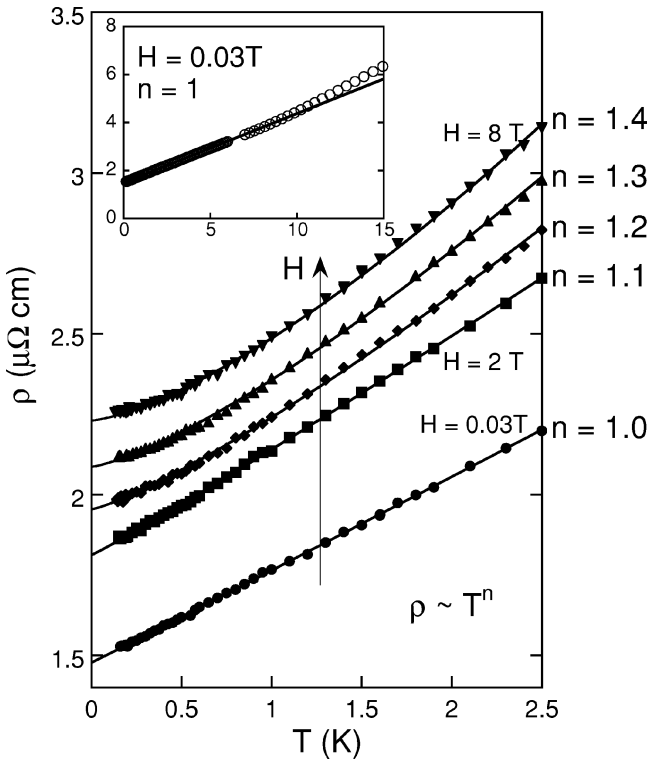

FIG. 6. Electrical resistivity ρ vs temperature T for $Ce_{0.6}Y_{0.4}RhIn_5$ at magnetic fields H between 0.03 and 8 T. The solid lines are fit to a power law temperature dependence $\rho \sim T^n$. Inset: ρ vs T at $H=0.03$T with an expanded temperature range.

ρ is linear with temperature from 150 mK to 10 K. The resistivity increases with magnetic field, and the data at all fields upto 8 T can be fit by a power law $\rho/\rho_0 = 1 - bT^n$. The power law exponent n increases linearly from $n=1$ for $H \sim 0$ to $n=1.4$ at $H=8$ T. At this rate, Fermi liquid behavior $(n=2)$ is expected in an applied magnetic field of $H=20$ T.

E. High-temperature data

In the electrical resistivity at higher temperatures, a crossover is observed from Kondo coherence to single-ion Kondo behavior at $x=0.8$. The resistivity $\rho(T)$ is shown for various $Ce_{1-x}Y_xRhIn_5$ samples in Fig. 7. For the samples with $0 \leqslant x \leqslant 0.5$ (main figure), a Kondo coherence shoulder occurs in the $\rho(T)$ data at $T \sim 50$ K. This shoulder is gradually suppressed in the samples with $x=0.6$ and $x=0.8$ and disappears by $x=0.9$ (inset). For the sample with $x=0.9$, an upturn in $\rho(T)$ at low temperatures, characteristic of the single-ion Kondo effect, is observed.

The magnetic susceptibility versus temperature is depicted in Fig. 8 where open symbols are for magnetic fields along the c axis and solid symbols are for fields within the ab plane. The magnetic susceptibility shows a strong anisotropy where χ_c is 2–3 times as large as χ_{ab}. This roughly corresponds to the anisotropy in the lattice, where the Ce interion distance along the c axis is almost twice as large as in the ab plane.

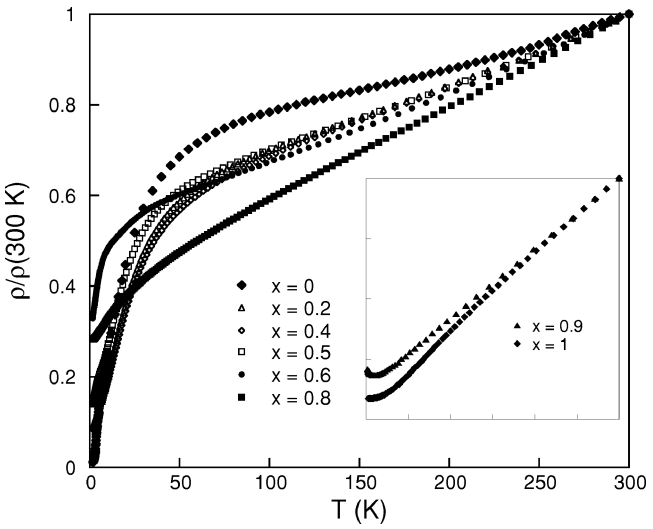

FIG. 7. Resistivity ρ normalized to its value at $T=300$ K vs temperature T for samples of $Ce_{1-x}Y_xRhIn_5$ with $0 \leqslant x \leqslant 0.8$. Inset shows $\rho/\rho(300\ \mathrm{K})$ vs T for samples with $x=0.9$ and $x=1.0$ with the same axes.

F. Phase diagram

The phase diagram of the $Ce_{1-x}Y_xRhIn_5$ system is displayed in Fig. 9. The Néel temperature T_N is determined from peaks in the specific heat and kinks in the resistivity and magnetic susceptibility.[8] T_N extrapolates to zero at a quantum critical point (QCP) near $x_c=0.38$. In the samples with $0.4 \leqslant x \leqslant 0.9$, the specific heat and magnetic susceptibility diverge with power law T dependences at low temperatures, characteristic of NFL behavior.

In the top right inset, the magnitudes of the NFL contribution to $C(T)$ and $\chi_{ab}(T)$ are shown. These magnitudes are plotted as A and B/λ where $\chi_{ab} = AT^{-1+\lambda}$ and $C(T)/T = BT^{-1+\lambda}$. In the magnetic susceptibility, the power law exponent λ is constant, so A is directly proportional to the magnitude of the NFL contribution to $\chi_{ab}(T)$. In the specific

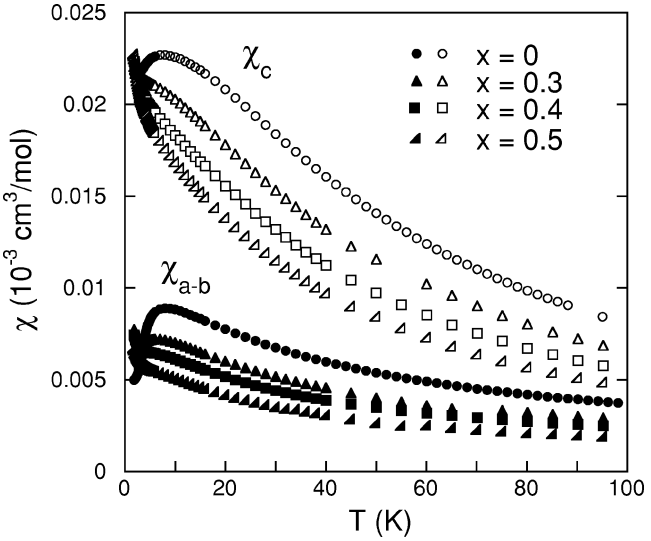

FIG. 8. Magnetic susceptibility vs T for fields aligned along the crystallographic ab plane, χ_{ab}, and c axis, χc.

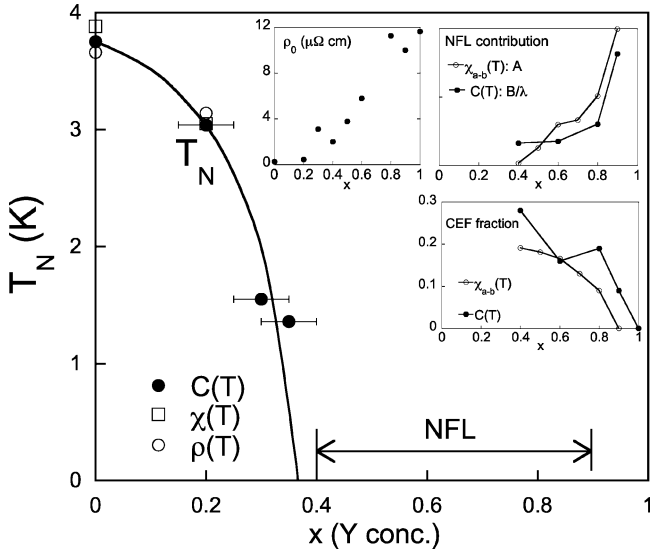

FIG. 9. Néel temperature T_N vs yttrium concentration x determined from the specific heat $C(T)$, magnetic susceptibility χ_{ab} and χ_c, and resistivity $\rho(T)$ for samples of $Ce_{1-x}Y_xRhIn_5$. The region of non-Fermi-liquid (NFL) behavior is indicated for samples with $0.4 \leqslant x \leqslant 0.9$. Upper left inset: resistivity at 1.8 K vs x. Upper right inset: magnitude of the NFL contributions to $C(T)$ (solid circles) and $\chi_{ab}(T)$ (open circles) plotted as B/λ and A where $C(T)/T = BT^{-1+\lambda}$ and $\chi_{ab} = AT^{-1+\lambda}$. Bottom inset: fraction of Ce ions contributing to the CEF-like effect in $C(T)$ (solid circles) and $\chi_{ab}(T)$ (open circles).

heat, the entropy under the NFL contribution to $C(T)$ is given by $S_{NFL} = \int C_{NFL}(T)/T dT = \int BT^{-1+\lambda}\, dT$, which is proportional to B/λ. The NFL contribution to both $C(T)$ and $\chi_{ab}(T)$ diverges with increasing x.

In the top left inset to Fig. 9, the resistivity at 1.8 K is plotted as a function of x. Above $x = 0.4$ the resistivity increases dramatically with x reaching a maximum at $YRhIn_5$ of $12 \mu\Omega$ cm.

The lower inset shows the fraction of Ce ions participating in the CEF-like effects in $C(T)$ and $\chi_{ab}(T)$ as a function of x. These fractions represent the amount by which the predicted CEF contribution to $C(T)$ and $\chi_{ab}(T)$ was reduced to fit the data. In both $C(T)$ and $\chi_{ab}(T)$, the CEF-like contribution is suppressed with increasing x. Thus, the specific heat and magnetic susceptibility are dominated by the CEF-like contributions in the vicinity of the QCP, but as the system moves away from the QCP, the NFL contribution increases in magnitude.

IV. DISCUSSION

A. NFL behavior

The $Ce_{1-x}Y_xRhIn_5$ system belongs to the growing class of compounds in which a magnetic ordering temperature is suppressed to 0 K by pressure or composition. In many of these systems, such as $CeIn_3$ and $U_{1-x}Y_xPd_2Al_3$,[5,19] NFL behavior occurs in the vicinity of the QCP and can be attributed to fluctuations of a magnetic order parameter at the QCP. However, in the $Ce_{1-x}Y_xRhIn_5$ system, the power law behavior in the specific heat and magnetic susceptibility is not in agreement with any quantum critical point theory. In fact, the NFL behavior becomes more pronounced with distance from the QCP.

One model which may be applicable to this system is the Griffiths-McCoy singularity model.[20] In this model, competition between the RKKY interaction and the Kondo effect in the presence of disorder in the magnetic lattice results in the formation of strongly coupled magnetic clusters with large susceptibilities. The magnetic susceptibility and specific heat are predicted to have power law T dependences. This model also requires a large magnetic anisotropy, which we observe in the magnetic susceptibility. The observed power law T dependences of $C(T)$ and $\chi_{ab}(T)$ agree well this model. However, the Griffiths-McCoy model predicts a single exponent λ such that $C(T)/T \sim \chi_{ab}(T) \sim T^{-1+\lambda}$. In the $Ce_{1-x}Y_xRhIn_5$ system, the power law exponent determined from the magnetic susceptibility, λ_χ, is constant at ~ 0.55, whereas the exponent determined from the specific heat, λ_C, varies from 0.8 to 0.3 with increasing x.

The fact that the magnitude of the NFL behavior increases with increasing distance from the QCP is unusual. One explanation is that close to the QCP, the CEF-like effect is competing with the NFL behavior. In this scenario the NFL contributions to $C(T)$ and $\chi(T)$ become larger with increasing distance from the QCP because the competing CEF-like effect is being suppressed.

Another possibility is that the NFL behavior is coupled to disorder, which is increasing with x. Usually, disorder due to random mixing of magnetic and nonmagnetic elements (e.g., Ce and Y) is expected to reach a maximum around 50% doping. However, in the $Ce_{1-x}Y_xRhIn_5$ system, the residual resistivity increases continuously, reaching a maximum at the end member $YRhIn_5$ compound (see top right inset of Fig. 9). Possibly the shrinking of the lattice due to the substitution of the smaller Y atom for Ce introduces significant amounts of scattering of the conduction electrons that overshadows any peak in the scattering rate caused by the disorder in the Ce-Y sublattice. The increase of the residual resistivity with x correlates with the increased NFL behavior; however, it is not possible to conclude whether the two phenomena are related. More experiments will be necessary to elucidate the nature of the NFL behavior in this system.

B. CEF-like features

The rounded features in $C_m(T)$ and $\chi_{ab}(T)$ [but not $\chi_c(T)$] above T_N are remarkably well fit by a CEF model with a consistent energy level scheme in which the Ce^{3+} $J = 5/2$ multiplet is split by the tetragonal crystal field into a magnetic Γ_6 doublet and two magnetic Γ_{t7} doublets. Fits to both $C_m(T)$ and $\chi_{ab}(T)$ yield the same energy level scheme. However, the magnitudes of the CEF-like contributions to $C_m(T)$ and $\chi_{ab}(T)$ are greatly reduced from the prediction, assuming 100% of the Ce ions in the material are contributing. Only 40% of the electrons would be participating in it at the QCP. Along these lines, the recovered entropy by 20 K is only $R \ln 2$, whereas $2R \ln 2$ is be expected since the Kondo

effect and the CEF splitting should each be contributing $R \ln 2$ to the entropy by 20 K. Another point to consider is that the features in $C_m(T)$ and χ_{ab} occur well below the Kondo coherence drop in the electrical resistivity ($\sim$50 K). Thus, to argue for the occurrence of CEF splitting, we must posit the existence of unscreened local moments around 4 K for a Kondo temperature greater than 50 K.

One way to resolve these discrepancies is to consider the effects of disorder. In a strongly disordered environment, some Ce ions could form local moments and exhibit energy level splitting by the CEF whereas others could be screened by the Kondo effect. The idea of unscreened moments well below the Kondo temperature has been explored before. In fact, it is a prerequisite for the Kondo disorder model for NFL theory,[18] in which disorder results in a distribution of Kondo temperatures with a finite number of unscreened moments existing even at zero temperature. The existence of a significant amount of disorder in the $Ce_{1-x}Y_xRhIn_5$ systems is supported by the very large values of the residual resistivity, as shown in Fig. 9. The reduced entropy ($R \ln 2$ instead of $2R \ln 2$) can be accounted for if each Ce ion only participates in one effect—CEF splitting or Kondo screening. In effect, the NFL behavior and the CEF-like behavior compete for electrons. This scenario is supported by the specific heat and magnetic susceptibility data; as NFL behavior becomes more pronounced with increasing x, the CEF-like bumps in $C(T)$ and $\chi(T)$ are suppressed, and the total entropy above 6 K is constant with x.

There are other possibilities for the origin of the rounded features in $C(T)$ and $\chi(T)$ other than CEF splitting, such as short-range magnetic order above T_N, spin-glass behavior, or even a partial gap in the density of states (DOS) such as has been observed in CeNiSn. Further measurements will be necessary to distinguish between these possibilities.

V. SUMMARY

We have investigated single-crystal samples of $Ce_{1-x}Y_xRhIn_5$ by means of specific heat, magnetic susceptibility, and resistivity measurements to low temperatures. The Néel temperature T_N is suppressed with increasing yttrium concentration and extrapolates to zero at $x_c \sim 0.38$. At low temperatures, the specific heat and magnetic susceptibility of the samples with $0.4 \leqslant x \leqslant 0.9$ exhibit NFL temperature dependences. After subtraction of features possibly due to CEF splitting, the specific heat and magnetic susceptibility can be fit by power law temperature dependences, reminiscent of the Griffiths-McCoy model for NFL behavior. A linear temperature dependence of the resistivity is observed at low temperatures for the sample with $x = 0.4$ and evolves towards $\rho \sim T^{1.4}$ as the applied magnetic field is increased to 8 T. The magnitude of the NFL contribution to $C(T)$ and $\chi_{ab}(T)$ becomes more pronounced with increasing x as the system moves away from the QCP, while the CEF-like contribution to $C(T)$ and $\chi_{ab}(T)$ dominates in the vicinity of the QCP and is suppressed with increasing x. Although NFL behavior extends to $x = 0.9$ in the specific heat and magnetic susceptibility, a crossover from Kondo coherence to single-ion Kondo behavior occurs in the resistivity between $x = 0.8$ and $x = 0.9$. Finally, entropy calculations reveal that the same electrons are participating in the antiferromagnetism, NFL, possible CEF splitting of the Ce^{3+} Hund's rule multiplet, and heavy electron behavior.

ACKNOWLEDGMENTS

This work was supported by the U.S. Department of Energy under Grant No. DE FG03-86ER-45230 and by the National Science Foundation under Grant No. DMR00-72125. We thank Dr. P. Allensbach for information regarding the tetragonal crystal field analysis.

*Permanent address: Emory University, Atlanta, GA 30322.

†Permanent address: Universität Karlsruhe, Germany.

[1] M.B. Maple, C.L. Seaman, D.A. Gajewski, Y. Dalichaouch, V.B. Barbetta, M.C. de Andrade, H.A. Mook, H.G. Lukefahr, O.O. Bernal, and D.E. MacLaughlin, J. Low Temp. Phys. **95**, 225 (1994).

[2] G.R. Stewart, Rev. Mod. Phys. **73**, 797 (2001).

[3] J.D. Thompson, R. Movshovich, Z. Fisk, F. Bouquet, N.J. Curro, R.A. Fisher, P.C. Hammel, H. Hegger, M.F. Hundley, M. Jaime, P.G. Pagliuso, C. Petrovic, N.E. Phillips, and J.L. Sarrao, J. Magn. Magn. Mater. **226-230**, 5 (2001).

[4] H. Hegger, C. Petrovic, E.G. Moshopoulou, M.F. Hundley, J.L. Sarrao, Z. Fisk, and J.D. Thompson, Phys. Rev. Lett. **84**, 4986 (2000).

[5] S.R. Julian, F.V. Carter, F.M. Grosche, R.K.W. Haselwimmer, S.J. Lister, N.D. Mathur, G.J. McMullan, C. Pfleiderer, S.S. Saxena, I.R. Walker, N.J.W. Wilson, and G.G. Lonzarich, J. Magn. Magn. Mater. **177-181**, 265 (1998).

[6] M.B. Maple, A. Amann, R.P. Dickey, E.J. Freeman, C. Sirvent, M.C. de Andrade, and N.R. Dilley, Physica B **281-282**, 332 (2000).

[7] V.S. Zapf, R.P. Dickey, E.J. Freeman, C. Sirvent, and M.B. Maple, Phys. Rev. B **65**, 024437 (2001).

[8] V.S. Zapf, E.J. Freeman, E.D. Bauer, J. Petricka, C. Sirvent, N.A. Frederick, R.P. Dickey, and M.B. Maple, Phys. Rev. B **65**, 014506 (2001).

[9] P.G. Pagliuso, C. Petrovic, R. Movshovich, D. Hall, M.F. Hundley, J.L. Sarrao, J.D. Thompson, and Z. Fisk, Phys. Rev. B **64**, 100503 (2001).

[10] C. Petrovic, R. Movshovich, M. Jaime, P.G. Pagliuso, M.F. Hundley, J.L. Sarrao, Z. Fisk, and J.D. Thompson, Europhys. Lett. **53**, 354 (2001).

[11] C. Petrovic, P. G. Pagliuso, M. F. Hundley, R. Movshovich, J. L. Sarrao, J. D. Thompson, Z. Fisk, and P. Monthoux, J. Phys.: Condens. Matter **13**, L337 (2001).

[12] T. Muramatsu, N. Tateiwa, T. Kobayashi, K. Shimizu, K. Amaya, D. Aoki, H. Shishido, Y. Haga, and Y. Onuki, J. Phys. Soc. Jpn. **70**, 3362 (2001).

[13] J.S. Kim, J. Alwood, G.R. Stewart, J.L. Sarrao, and J.D. Thompson, Phys. Rev. B **64**, 134524 (2001).

[14] W. Bao, P.G. Pagliuso, J.L. Sarrao, J.D. Thompson, Z. Fisk, J.W. Lynn, and R.W. Erwin, Phys. Rev. B **62**, R14 621 (2000).

[15] N.J. Curro, P.C. Hammel, P.G. Pagliuso, J.L. Sarrao, J.D. Thompson, and Z. Fisk, Phys. Rev. B **62**, R6100 (2000).

[16] G. Fischer and A. Herr, Phys. Status Solidi B **141**, 589 (1987).
[17] K.W. Stevens, Proc. Phys. Soc., London, Sect. A **65**, 209 (1952).
[18] E. Miranda, V. Dobrosavljevic, and G. Kotliar, J. Phys.: Condens. Matter **8**, 9871 (1996).
[19] E.J. Freeman, M.C. de Andrade, R.P. Dickey, N.R. Dilley, and M.B. Maple, Phys. Rev. B **58**, 16 027 (1998).
[20] A.H. Castro Neto, G. Castilla, and B.A. Jones, Phys. Rev. Lett. **81**, 3531 (1998).